Particulate counter electrode system for enhanced light harvesting in dye-sensitized solar cells

Kyoseung Sim,[1] Shi-Joon Sung,[1,*] Si-Nae Park,[2] Dae-Hwan Kim,[1] Jin-Kyu Kang[2]

[1]*Green Energy Research Division, Daegu Gyeongbuk Institute of Science and Technology (DGIST), 50-1, Sang-ri, Hyeonpung-myeon, Dalseong-gun, Daegu, 711-873, South Korea*

[2]*Advanced Convergence Research Center, Daegu Gyeongbuk Institute of Science and Technology (DGIST), 50-1, Sang-ri, Hyeonpung-myeon, Dalseong-gun, Daegu, 711-873, South Korea*

[*]*sjsung@dgist.ac.kr*

Abstract: A particulate counter electrode with photo scattering and redox catalytic properties is applied to dye sensitized solar cells (DSSCs) in order to improve photo conversion efficiency and simplify the assembly process. Our particulate counter electrode acts as both a photo reflecting layer and a catalyst for reduction of electrolyte. The reflective and catalytic properties of the electrode are investigated through optical and electrochemical analysis, respectively. A short circuit current density enhancement is observed in the DSSCs without the need to add an additional reflecting layer to the electrode. This leads to a simplified assembly process.

OCIS codes: (350.6050) Solar energy; (160.4670) Optical materials.

References and links

1. B. O'Regan and M. Grätzel, "A low-cost, high-efficiency solar cell based on dye-sensitized colloidal TiO_2 films," Nature **353**(6346), 737–740 (1991).
2. A. Burke, L. Schmidt-Mende, S. Ito, and M. Grätzel, "A novel blue dye for near-IR 'dye-sensitized' solar cell applications," Chem. Commun. (Camb.) **3**, 234–236 (2006).
3. T. Yamaguchi, Y. Uchida, S. Agatsuma, and H. Arakawa, "Series-connected tandem dye-sensitized solar cell for improving efficiency to more than 10%," Sol. Energy Mater. Sol. Cells **93**(6–7), 733–736 (2009).
4. M. A. Green, K. Emery, Y. Hishikawa, W. Warta, and E. D. Dunlop, "Solar cell efficiency tables (version 41)," Prog. Photovolt. Res. Appl. **21**(1), 1–11 (2013).
5. S. Kurtz and J. Geisz, "Multijunction solar cells for conversion of concentrated sunligh to electricity," Opt. Express **18**(S1), A73–A78 (2010).
6. M. Wiemer, V. Sabnis, and H. Yuen, "43.5% efficient lattice matched solar cells," Proc. SPIE **8108**, 810804 (2011).
7. D. W. Liu, I. C. Cheng, J. Z. Chen, H. W. Chen, K. C. Ho, and C. C. Chiang, "Enhanced optical absorption of dye-sensitized solar cells with microcavity-embedded TiO_2 photoanodes," Opt. Express **20**(Suppl 2), A168–A176 (2012).
8. A. K. Chandiran, N. Tetreault, R. Humphry-Baker, F. Kessler, E. Baranoff, C. Yi, M. K. Nazeeruddin, and M. Grätzel, "Subnanometer Ga_2O_3 tunneling layer by atomic layer deposition to achieve 1.1 V open-circuit potential in dye-sensitized solar cells," Nano Lett. **12**(8), 3941–3947 (2012).
9. Y. Jhang, Y. Tsai, C. Tsai, S. Hsu, T. Huang, C. Lu, M. Chen, Y. Chen, and C. Wu, "Nanostructured platinum counter electrodes by self-assembled nanospheres for dye-sensitized solar cells," Org. Electron. **13**(10), 1865–1872 (2012).
10. A. Yella, H. W. Lee, H. N. Tsao, C. Yi, A. K. Chandiran, M. K. Nazeeruddin, E. W. Diau, C. Y. Yeh, S. M. Zakeeruddin, and M. Grätzel, "Porphyrin-sensitized solar cells with cobalt (II/III)-based redox electrolyte exceed 12 percent efficiency," Science **334**(6056), 629–634 (2011).
11. Q. Xu, F. Liu, W. Meng, and Y. Huang, "Plasmonic core-shell metal-organic nanoparticles enhanced dye-sensitized solar cells," Opt. Express **20**(S6), A898–A907 (2012).
12. J. Y. Lee, S. Lee, J. K. Park, Y. Jun, Y. G. Lee, K. M. Kim, J. H. Yun, and K. Y. Cho, "Simple approach for enhancement of light harvesting efficiency of dye-sensitized solar cells by polymeric mirror," Opt. Express **18**(Suppl 4), A522–A527 (2010).
13. K. Lee, J. Yun, Y. Han, J. Yim, N. Park, K. Cho, and J. Park, "Enhanced light harvesting in dye-sensitized solar cells with highly reflective TCO- and Pt-less counter electrodes," J. Mater. Chem. **21**(39), 15193–15196 (2011).
14. M. Marszalek, S. Nagane, A. Ichake, R. Humphry-Baker, V. Paul, S. M. Zakeeruddin, and M. Grätzel, "Tuning spectral properties of phenothiazine based donor–p–acceptor dyes for efficient dye-sensitized solar cells," J. Mater. Chem. **22**(3), 889–894 (2011).

#186154 - $15.00 USD Received 28 Feb 2013; revised 17 Apr 2013; accepted 25 Apr 2013; published 6 May 2013

15. A. Mihi, M. E. Calvo, J. A. Anta, and H. Míguez, "Spectral response of opal-based dye-sensitized solar cells," J. Phys. Chem. C **112**(1), 13–17 (2008).
16. Z. Zhang, L. Zhang, M. N. Hedhili, H. Zhang, and P. Wang, "Plasmonic gold nanocrystals coupled with photonic crystal seamlessly on TiO_2 nanotube photoelectrodes for efficient visible light photoelectrochemical water splitting," Nano Lett. **13**(1), 14–20 (2013).
17. Y. Ee, R. A. Arif, N. Tansu, P. Kumnorkaew, and J. F. Gilchrist, "Enhancement of light extraction efficiency of InGaN quantum wells light-emitting diodes using SiO_2/polystyrene microlens arrays," Appl. Phys. Lett. **91**(22), 221107 (2007).
18. P. Kumnorkaew, Y. K. Ee, N. Tansu, and J. F. Gilchrist, "Investigation of the deposition of microsphere monolayers for fabrication of microlens arrays," Langmuir **24**(21), 12150–12157 (2008).
19. W. Koo, W. Youn, P. Zhu, X. Li, N. Tansu, and F. So, "Light extraction of organic light emitting diodes by defective hexagonal-close-packed array," Adv. Funct. Mater. **22**(16), 3454–3459 (2012).
20. M. A. Tsai, H. W. Han, Y. L. Tsai, P. C. Tseng, P. Yu, H. C. Kuo, C. H. Shen, J. M. Shieh, and S. H. Lin, "Embedded biomimetic nanostructures for enhanced optical absorption in thin-film solar cells," Opt. Express **19**(Suppl 4), A757–A762 (2011).
21. J. Zhao, B. Sun, L. Qiu, H. Caocen, Q. Li, X. Chen, and F. Yan, "Efficient light-scattering functionalized TiO_2 photoanodes modified with cyanobiphenyl-based benzimidazole for dye-sensitized solar cells with additive-free electrolytes," J. Mater. Chem. **22**(35), 18380–18386 (2012).
22. Y. Park, Y. Chang, B. Kum, E. Kong, J. Son, Y. Kwon, T. Park, and H. Jang, "Size-tunable mesoporous spherical TiO_2 as a scattering overlayer in high-performance dye-sensitized solar cells," J. Mater. Chem. **21**(26), 9582–9586 (2011).
23. F. Huang, D. Chen, X. L. Zhang, R. A. Caruso, and Y. Cheng, "Dual-function scattering layer of submicrometer-sized mesoporous TiO_2 beads for high-efficiency dye-sensitized solar cells," Adv. Funct. Mater. **20**(8), 1301–1305 (2010).
24. D. Wu, F. Zhu, J. Li, H. Dong, Q. Li, K. Jiang, and D. Xu, "Monodisperse TiO_2 hierarchical hollow spheres assembled by nanospindles for dye-sensitized solar cells," J. Mater. Chem. **22**(23), 11665–11671 (2012).
25. W. Jiang, L. Yin, H. Liu, and Y. Ding, "Nanograss-structured counter electrode for dye-sensitized solar cells," J. Power Sources **218**, 405–411 (2012).
26. W. S. Chi, J. W. Han, S. Yang, D. K. Roh, H. Lee, and J. H. Kim, "Employing electrostatic self-assembly of tailored nickel sulfide nanoparticles for quasi-solid-state dye-sensitized solar cells with Pt-free counter electrodes," Chem. Commun. (Camb.) **48**(76), 9501–9503 (2012).
27. T. Zhang, H. Chen, C. Su, and D. Kuang, "A novel TCO- and Pt-free counter electrode for high efficiency dye-sensitized solar cells," J. Mater. Chem. **1**(5), 1724–1730 (2013).
28. E. Ramasamy and J. Lee, "Ferrocene-derivatized ordered mesoporous carbon as high performance counter electrodes for dye-sensitized solar cells," Carbon **48**(13), 3715–3720 (2010).
29. J. Kim and S. Rhee, "Counter electrode system of Pt on stainless steel (SS) for electron injection into iodide redox couple," J. Electrochem. Soc. **159**(1), B6–B11 (2012).
30. K. Sim, S. Sung, and D. Kim, "Light harvest properties of dye-sensitized solar cells with different spatial configurations of reflecting layer," J. Nanosci. Nanotechnol. (to be published).
31. K. S. Kim, H. Song, S. H. Nam, S. M. Kim, H. Jeong, W. B. Kim, and G. Y. Jung, "Fabrication of an efficient light-scattering functionalized photoanode using periodically aligned ZnO hemisphere crystals for dye-sensitized solar cells," Adv. Mater. **24**(6), 792–798 (2012).

1. Introduction

Dye sensitized solar cells (DSSCs) were first developed by Grätzel in 1991 [1] and are a promising system for next generation solar cells. DSSCs have attracted enormous attention due to their variable absorption through organic absorbers [2,3] and high efficiency under low light conditions as well as normal photo intensity. However, the photo conversion efficiency of DSSCs is still well below that of traditional inorganic-based solar cells formed of chalcogenide compounds or amorphous silicon [4,5]. Moreover, recent works on multi-junction tandem cells using GaInP/GaAs/GaInNAs had resulted in high performance and record photo-current conversion efficiency more than 43.5% [6]. In order to overcome these stagnation of DSSCs performance and relatively lower property than inorganic based solar cells, many research groups have attempted to increase DSSC device performance through enhancement of the short-circuit current density (J_{sc}), open-circuit voltage (V_{oc}), and fill factor (FF) [7–10].

In DSSCs, J_{sc} is one of the key device performance indicators. J_{sc} is closely linked to the light harvesting capacity of the photo absorber, which depends on the molar absorption coefficient, the amount of absorbent loading and the intensity of light incident on the active layer [11–14]. The light harvesting ability of the DSSCs can be improved by increasing the intensity of incident light. This can be done through the addition of a reflecting or scattering layer, such as a photonic crystal layer [15,16]. This photonic crystal could be made using

#186154 - $15.00 USD Received 28 Feb 2013; revised 17 Apr 2013; accepted 25 Apr 2013; published 6 May 2013

rapid convective deposition (RCD) [17,18], which was applied various electronic devices such as organic light-emitting diodes [19] and solar cells [20]. In addition, a bilayer photoanodes is one of the widely adapted scattering layers [21–24]. Although these additional layers result in an improved J_{sc}, they are disadvantageous due to the extra fabrication steps required when manufacturing the DSSCs. These scattering and reflecting layers are now almost always included in DSSCs due to the J_{sc} enhancement they provide.

Structurally engineered counter electrodes can also be used to improve the light harvesting properties of DSSCs. Structured electrodes have both reflecting and catalytic properties [25], meaning that additional scattering and reflecting layers are not needed. Structurally engineered electrodes are, however, more elaborate and therefore complicated to form. In this paper, we report a novel particulate counter electrode with photo scattering and redox catalytic properties. This particulate counter electrode does not require additional manufacturing steps.

Our particulate counter electrode is composed of large TiO_2 particles and Pt particles. The reflective and catalytic properties are investigated through optical and electrochemical analysis, respectively. The optimal composition of the particulate counter electrode for high efficiency DSSCs is discussed. Electrical, optical, and electrochemical measurements are used to confirm that our particulate counter electrode increases J_{sc} without the need to deposit an additional reflective or scattering layer. The result is an improvement in device performance and a simplified fabrication process.

2. Experimental methods

Conventional sandwich configuration DSSCs, consisting of a working electrode and a counter electrode, were fabricated. The DSSCs were made with conventional counter electrode and our particulate counter electrode. Figure 1 shows the geometry of DSSCs and the path of incident photons.

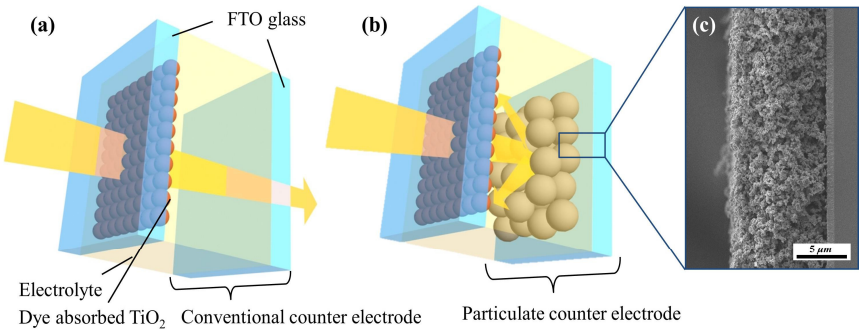

Fig. 1. Schematic diagrams of the DSSCs with (a) conventional counter electrode and (b) particulate counter electrode. The path of incident photons is shown by the arrows for each solar cell. (c) Cross-section SEM image of particulate counter electrode.

The working electrode was formed from fluorine-doped tin oxide (FTO), resulting in a transparent conductive electrode (Pilkington, ~8 Ω/sq). The FTO surface was cleaned using the following procedure: step-wise ultrasonic treatment in detergent, DI-water, acetone, and 2-propanol for 15 min at room temperature. A TiO_2 paste containing 20 nm sized particles (Solaronix, T/SP) was deposited onto the cleaned FTO substrate, via blade coating, to form a transparent, porous titanium oxide film. The doctor-blading process was repeated twice. The blade coated TiO_2 film was sintered in air at 500°C for 60 min. To maintain adhesion between the TiO_2 nanoparticles in the porous film, the film was treated with 40 mM $TiCl_4$ in a dry oven at 70°C for 30 min. The samples were then rinsed with DI-water and ethanol, and sintered in air at 500°C for 60 min. The edges of the sample were subsequently trimmed. To form the solar cell device the TiO_2 film was first immersed in a 0.3-mM N719 dye (Solaronix) solution, consisting of an acetonitrile and *tert*-butanol mixture (50:50 vol%), at room

#186154 - $15.00 USD Received 28 Feb 2013; revised 17 Apr 2013; accepted 25 Apr 2013; published 6 May 2013

temperature for 24 h. The dye-adsorbed TiO_2 film was then rinsed with acetonitrile and dried at 70°C for about 10 min. The active area of the sample was determined by microscopy (Olympus SZ61) and the iSolution-NFR Lite software. The active area ranged from 0.285 to 0.296 cm^2.

Conventional counter electrodes were prepared using a thermal reduction method. An H_2PtCl_6 solution was deposited via spin coating onto cleaned FTO glass with 0.7 mm holed and then heated at 450°C for 60 min.

To form the particulate counter electrode, TiO_2 particle paste (Solaronix, R/SP) was blended with H_2PtCl_6 solution at a ratio of 0.2 ml of H_2PtCl_6 solution per gram of TiO_2 paste. The following H_2PtCl_6 solution concentrations were used electrode A: 0.001 M, electrode B: 0.01 M, electrode C: 0.1 M, electrode D: 1.0 M. This blended paste was blade coated onto cleaned 0.7 mm holed FTO and then sintered at 450°C for 60 min. The same sintering process was used for both the conventional counter electrode and the particulate counter electrode.

Devices were assembled from the working and counter electrodes above. A 60 μm thick layer of thermoplastic sealant (Surlyn, Solaronix SX1170-60) was used as a spacer for the two electrodes. The inside of the cell was filled with a liquid electrolyte containing 0.03 M iodine, 1 M 1-methyl-3-propylimidazolium iodide, 0.1 M guanidine thiocyanate, and 0.5 M *tert*-butyl pyridine. The solvent used was acetonitrile/valeronitrile with a 85/15 vol% ratio.

The morphology of the particulate counter electrodes was imaged using scanning electron microscopy (SEM). The reflectance spectra of the particulate counter electrodes were measured using a Varian Cary 5000 spectrometer with an integrating sphere. A potentiostat (Ivium, IviumStat) was used to perform cyclic voltammetry (CV) measurements. The CV tests were carried out in a three-electrode system. The particulate counter electrode, Pt mesh, and Ag+/AgCl 1 M were used for the working, counter, and reference electrodes, respectively. The supporting electrolyte was a mixture of 5 mM iodine (Aldrich) and 5 mM lithium iodide (LiI, Aldrich) in acetonitrile containing 0.1 M tetrabutyl ammonium hexafluorophosphate (TBA-PF_6, Aldrich). The CV measurements were carried out over a voltage range of −0.3 V to + 1.0 V at a scan rate of 0.05 V/s. A potentiostat was used to measure the electrochemical impedance of FTO/Pt/electrolyte/particulate counter electrode dummy cells over the frequency range of 100 kHz to 0.1 Hz at amplitude of 0.01V. The photo current density vs. voltage curves of the devices were measured under AM 1.5 light conditions using a Keithley 2400 source meter and a solar simulator equipped with a 1-kW xenon arc lamp (ORIEL, Newport). A standard silicon solar cell (PV Measurement Inc.) was used to calibrate the power of the AM 1.5 simulated light (100 mW/cm^2). The incident photon to current conversion efficiency (IPCE) was measured using a PEC-S20 action spectrum measurement system (Peccell Technologies Inc.). The light intensity of this system was calibrated using a Hamamatsu S1337-1010BQ Si photodiode.

3. Results and discussion

Figure 2(a) shows a photograph of TiO_2 R/SP film and the particulate counter electrodes (electrode A to electrode D). The darker layers correspond to TiO_2 films containing higher concentrations of H_2PtCl_6. The photo reflective properties of the particulate counter electrode were studied by measuring the UV-vis reflection spectra. As shown in Fig. 2(b), pristine TiO_2 R/SP film that does not contain H_2PtCl_6 solution has highest reflectance. However, as the H_2PtCl_6 solution concentration in TiO_2 particle paste increased the reflectance of the particulate counter electrodes decreased. These results show that replacing the counter electrode with the particulate counter electrode leads to an enhancement of the light harvesting properties and we can easily control the reflectance of counter electrode by controlling the H_2PtCl_6 solution concentration in TiO_2 particle paste.

#186154 - $15.00 USD Received 28 Feb 2013; revised 17 Apr 2013; accepted 25 Apr 2013; published 6 May 2013

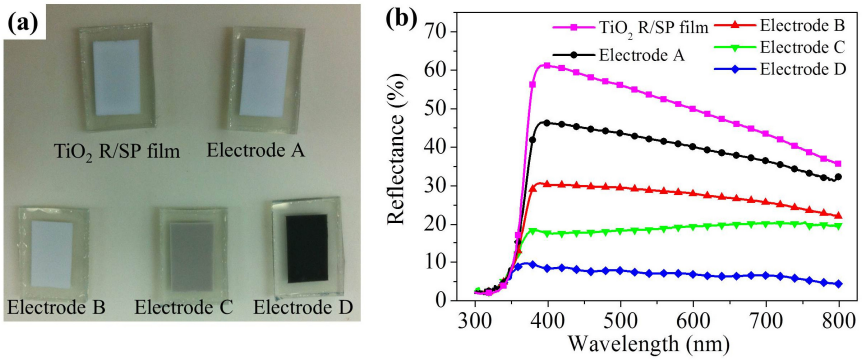

Fig. 2. (a) Photograph showing the particulate counter electrodes prepared from the mixture of TiO_2 R/SP paste and H_2PtCl_6 solution. The mixture of TiO_2 R/SP paste and H_2PtCl_6 solution with different concentration (Electrode A: 0.001M, Electrode B: 0.01M, Electrode C: 0.1M, Electrode D: 1.0M) was deposited on FTO by doctor blading and sintered at 450 °C for 60 min. (b) UV-vis reflectance spectra of the various particulate counter electrodes (electrode A to electrode D) and R/SP film.

Figure 3(a) shows the CV measurements of the particulate counter electrodes. The spectra show two pairs of redox peaks. The more negative pair of peaks results from the redox reaction given in Eq. (1) and the more positive pair from the redox reaction given in Eq. (2) [26].

$$I_3 + 2e^- \leftrightarrow 3I^-, \quad (1)$$

$$3I_2 + 2e^- \leftrightarrow 2I_3^-. \quad (2)$$

On the counter electrode, Pt serves as a catalyst for the chemical reduction of tri-iodine to iodide. Two parameters are used to evaluate the catalytic activity of the counter electrode. The first is the peak current density, which gives information about the catalytic activity and allows the reactivity to be compared [27]. The maximum current density is found from the peak in the chemical reduction described in Eq. (1). The second parameter is the peak-to-peak separation (ΔE_p). This is inversely proportional to the electrochemical constant k_s ($\Delta E_p \propto 1/k_s$). A smaller ΔE_p therefore represents a higher catalytic activity [28].

As shown in Fig. 3(a), electrode A has the lowest current density. A successive increase in the current density is seen from electrodes A to D. Electrode D has the lowest ΔE_p of 260mV. The value of ΔE_p for electrodes C and B are higher than that of D at 425 mV and 515 mA, respectively. The value of ΔE_p for electrode A was hard to determine due to a poorly defined second peak. The high catalytic performance of electrode D suggests that it is most suitable for the counter electrode. Electrodes B and C are not unsuitable due to their appropriate catalytic activity and electrode A is not suitable for use in DSSCs because low catalytic reactivity.

In order to estimate the catalytic activity at the particulate counter electrode, EIS measurements were carried out. A dummy cell, aforementioned in experimental section, was used for the measurements. Conventional Nyquist plots of the cells are shown in Fig. 3(b). The highest-frequency intercept on the real axis gives the series resistance (R_s) of the cell, R_s is induced by sheet resistance of the electrode. The highest-frequency arc gives the electrochemical reaction resistance (R_{ct}) of the redox coupling at the electrode, and the low-frequency arc gives the Warburg impedance (W_s) of the redox species [29]. From Fig. 3(b) it can be seen that the values of R_s for the four particulate counter electrodes are the same (electrode A: 15.05 Ω, electrode B: 14.39 Ω, electrode C: 14.7 Ω, electrode D: 14.45 Ω). The similar values of R_s are a result of the same FTO substrate being used for each electrode. A difference in R_{ct}, however, is observed. Electrode D has the lowest R_{ct} (17.45 Ω) and electrode A the largest. The data show that the degree of catalytic activity increases with increasing

#186154 - $15.00 USD Received 28 Feb 2013; revised 17 Apr 2013; accepted 25 Apr 2013; published 6 May 2013

H_2PtCl_6 concentration in the TiO_2 film. This result corresponds well with the CV measurements.

The results from the CV and EIS measurements show that, apart from electrode A, the particulate counter electrodes can be used as counter electrodes in DSSCs.

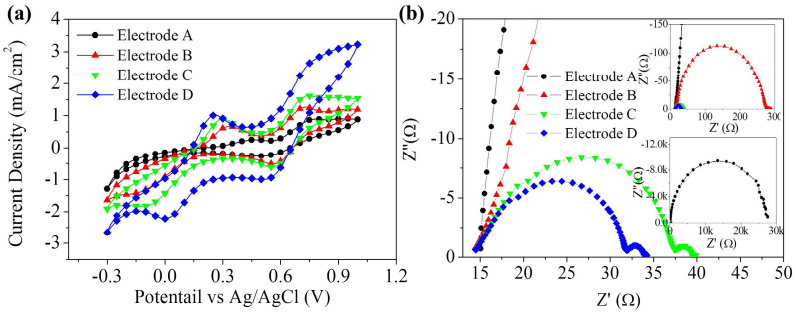

Fig. 3. (a) Cyclic voltammograms for the four particulate counter electrodes. (b) Electrochemical impedance spectra of the dummy cells. The scan rate in (a) is 50 mV/s. The insets in (b) show the same EIS data at different magnifications.

To understand the origin of the catalytic properties of the particulate counter electrodes, the surface morphology was investigated using field-emission scanning electron microscopy (FE-SEM). The SEM images can be seen in Fig. 4. As expected, all electrodes have a particulate morphology. For electrode D, small particles are seen to form on top of the larger particles. Because no small particles are observed in the SEM images for electrode A due to the low H_2PtCl_6 solution concentration used in their formation, we could conclude that these small particles are composed of Pt. Therefore, it is most likely that the darkening of the particulate counter electrodes observed in Fig. 1 arises from the increased presence of the small Pt particles. In order to probe the origin of catalytic properties of the particulate counter electrodes more distinctly, the particulate layer was removed from the FTO substrate, which was then imaged separately [Figs. 4(e)–4(h)]. For electrode D [Fig. 4(h)], the small particles seen on the FTO substrate are formed of Pt. In general TiO_2 is not a conductive material. It is therefore most likely that the catalytic properties of the particulate counter electrodes arise from the presence of the Pt particles on the FTO. In our previous study, we showed that an R/SP electrode formed on Pt coated FTO substrate acts as a proper counter electrode [30]. This supports the conclusion that catalytic redox reactions can occur at Pt inside our porous particulate counter electrode. Hence, we could find out that the higher H_2PtCl_6 solution concentration used to make the blended paste for formation of particulate counter electrode has a lower reflectance and a higher catalytic activity the resulting particulate counter electrode.

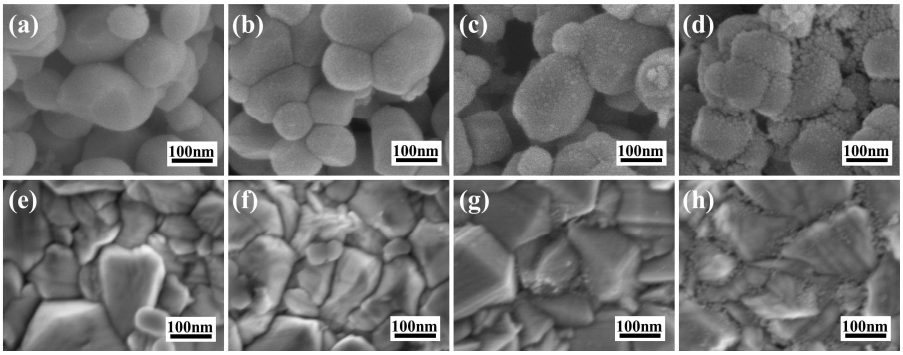

Fig. 4. FE-SEM images of the particulate counter electrodes (a) electrode A, (b) electrode B, (c) electrode C, and (d) electrode D, and the underlying FTO substrates (e) electrode A, (f) electrode B, (g) electrode C, and (h) electrode D. The scale bar is 100 nm.

#186154 - $15.00 USD Received 28 Feb 2013; revised 17 Apr 2013; accepted 25 Apr 2013; published 6 May 2013

To evaluate the performance of DSSCs made from our particulate counter electrodes (devices B, C, and D), current density vs. voltage measurements were carried out. For the purpose of comparison, a reference device was made from a Pt coated FTO counter electrode (Reference). As shown in Fig. 5(a) and Table 1, the devices all have a similar V_{oc} but different J_{sc} and FF. As a result, different photocurrent conversion efficiency is measured for each device. The high J_{sc} measured for device B results from the high reflectance of electrode B. However, its low catalytic activity results in a low FF and low photocurrent conversion efficiency (4.65%). No difference is seen in the J_{sc} measured for device D and reference device. A small increase in FF is however seen due to the low reflectance and high catalytic properties of electrode D. These properties lead to little improved photocurrent conversion efficiency for device D (7.44%), as compared with that of reference device (7.31%). Device C is seen to have the best performance. For device C, the slight decrease observed in FF is offset by a significant enhancement in J_{sc} resulting in a photocurrent conversion efficiency of 7.96%.

The IPCE spectra give further evidence of the optical contribution of our particulate counter electrodes [Fig. 5(b)]. The maximum IPCE values at 530 nm are 66.4%, 72.8%, 70.1% and 66.9% for reference device, device B, C, and D, respectively. Devices B and C both have a noticeably enhanced IPCE from 500 nm to 750 nm, while devices D and reference have similar IPCE spectra. This behavior corresponds with the trend seen in the J_{sc} values [Fig. 5(a)] and reflectance spectra of the different electrodes [Fig. 2(b)].

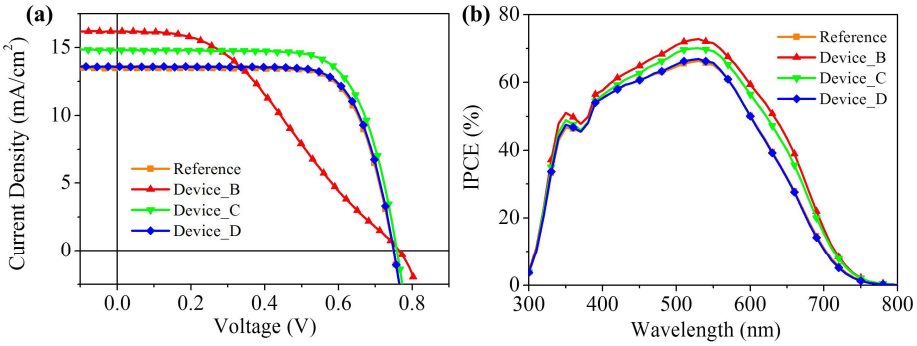

Fig. 5. (a) Graph showing the current density as a function of voltage for devices B, C, D, and reference. (b) Graph showing the IPCE spectra as a function of wavelength for devices B, C, D, and reference.

Table 1. Electrical Properties of the DSSC Devices

Device	V_{oc} (V)	J_{sc} (mA/cm^2)	FF	η (%)
reference	0.749	13.484	72.40	7.31
device B	0.764	16.197	37.55	4.65
device C	0.756	14.808	71.10	7.96
device D	0.750	13.582	73.04	7.44

In order to investigate the internal resistance of the devices EIS experiments were carried out. Figure 6(a) shows representative Nyquist plots for the devices, it show conventional three distinct semicircles. The highest-frequency intercept on the real axis represents the overall series resistance (R_s). The high-frequency (>kHz) semicircle gives the electrochemical reaction resistance of the counter electrode (R_{ct1}). The intermediate-frequency (1 Hz–1 kHz) semicircle gives the charge transport resistance at the TiO_2/dye/electrolyte interfaces (R_{ct2}). The Warburg diffusion process in the electrolyte can be found from the low-frequency (<1 Hz) semicircle. These definitions are the widely used conventional interpretations [31]. The EIS data for the different devices show similar features however, there are a number of differences. The factors that significantly vary are R_{ct1} and R_{ct2}. The value of R_{ct1} is 4.12 Ω, 6.26 Ω, and 2.23 Ω, for reference devices, C, and D, respectively. Device B has a very large R_{ct1} due to its low catalytic properties, as discussed earlier. A comparison of the R_{ct1} values for

#186154 - $15.00 USD Received 28 Feb 2013; revised 17 Apr 2013; accepted 25 Apr 2013; published 6 May 2013

the reference, device C, and D shows that the different FF values shown in Table 1 are caused by the catalytic behavior of counter electrodes. The value of R_{ct2} is 17.75 Ω, 15.10 Ω, and 17.28 Ω for reference device, device C, and D, respectively. The value of R_{ct2} for device B could not be determined due to screening of the high-frequency semicircle by the intermediate-frequency semicircle. The low R_{ct2} for device C indicates that more free electrons are produced during light harvesting and is in agreement with the increased reflectance, J_{sc} and IPCE observed for this device [31].

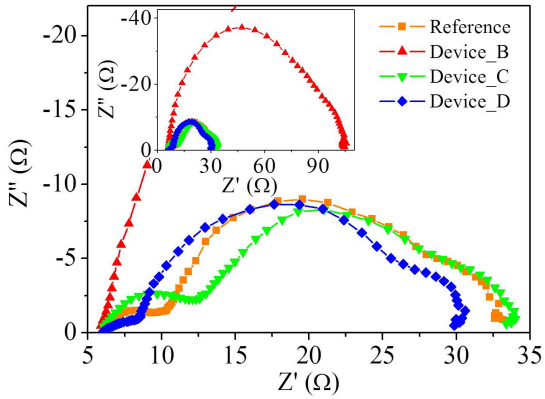

Fig. 6. Nyquist plots of devices B, C D, and reference under 1 sun illumination. The inset shows a magnification of the data.

4. Conclusions

In summary, we proposed a novel, easy to make, particulate counter electrode for use in DSSCs. These particulate counter electrodes were formed of large TiO_2 particles blended with the Pt precursor H_2PtCl_6. The TiO_2/H_2PtCl_6 blends were sintered to form porous films on FTO substrates. Optical characterization of the electrodes showed that their reflectance was inversely proportional to their catalytic performance, which in turn was dependent on the ratio of R/SP to H_2PtCl_6 used to form the porous film. The optimal TiO_2/H_2PtCl_6 blend that showed both light harvest enhancement and no significant decline in FF was found. Comparison of devices formed from our particulate counter electrodes, and those formed from standard Pt electrodes, indicated that the use of our electrodes in DSSCs leads to an increased photocurrent conversion efficiency. The results of this study suggest that particulate counter electrode DSSCs are a potential candidate for low-cost solar power systems. These systems would have enhanced device performance and require no additional light capture enhancement layers, making them simpler and cheaper to make.

Acknowledgments

This work was supported by the DGIST R&D Program of the Ministry of Education, Science and Technology of South Korea (13-EN-04) and by a grant from the Fundamental R&D program for Core Technology of Materials (10037239) funded by the Ministry of Knowledge Economy, South Korea.

#186154 - $15.00 USD Received 28 Feb 2013; revised 17 Apr 2013; accepted 25 Apr 2013; published 6 May 2013